

Near-field for electrodynamics at sub-wavelength scales: Generalizing to an arbitrary number of dielectrics

Shaohong Li,^{1,2} Yi Gao,² and Daniel Neuhauser^{2,a)}

¹*School of Chemistry and Chemical Engineering, Nanjing University, Nanjing, Jiangsu 210093, China*

²*Department of Chemistry and Biochemistry, University of California at Los Angeles, Los Angeles, California 90095-1569, USA*

(Received 12 February 2012; accepted 18 May 2012; published online 18 June 2012)

We extend the recently developed near-field (NF) method to include an arbitrary number of dielectrics. NF assumes that the dipoles and fields respond instantaneously to the density, without retardation. The central task in NF is the solution of the Poisson equation for every time step, which is here done by a conjugate gradient method which handles any dielectric distribution. The optical response of any metal-dielectric system can now be studied very efficiently in the near field region. The improved NF method is first applied to simple benchmark systems: a gold nanoparticle in vacuum and embedded in silica. The surface plasmons in these systems and their dependence on the dielectrics are reproduced in the new NF approach. As a further application, we study a silver nanoparticle-based structure for the optical detection of a “lipid” (i.e., dielectric) layer in water, where the layer is wrapping around part of the metallic nanostructure. We show the ~ 0.1 - 0.15 eV shift in the spectrum due to the presence of the layer, for both spherical and non-spherical (sphere+rod) systems with various polarizations. © 2012 American Institute of Physics. [<http://dx.doi.org/10.1063/1.4726076>]

I. INTRODUCTION

There is much interest in the optical properties of metallic nanostructures with sizes below 50 nm,¹⁻³ due to their potential applications in bio-sensing,^{4,5} optoelectronics,⁶ and photo-chemistry.^{7,8} Theoretically, there has also been much effort for understanding electrodynamics of metallic nanostructures⁹⁻¹³ and the mechanism of their dynamic coupling to nearby molecules¹⁴⁻²⁰ at sub-wavelength scales.

Recently we developed the near-field (NF) method,²¹ which quantitatively studies electrodynamics of nanostructures at sub-wavelength scales. When the size of the nanostructure is much smaller than the optical wavelength, retardation effects can be neglected. Then, the longitudinal component of electric field dominates so that the field is a gradient of an instantaneous scalar potential which fulfills the Poisson equation. NF therefore studies only the time-propagation of the longitudinal electric field, ignoring the transverse terms. The main advantage of NF is that the time step used for the evolution of electric field can be as high as a few atomic units, hundreds of times larger than that required in the Yee-type Maxwell finite-difference time-domain approach²² for sub-nanometer scales.

In NF, at each time step a Poisson equation has to be solved. If there are no dielectrics (i.e., no semiconductor and insulators) or there is only a single dielectric without vacuum, the Poisson equation can be solved by an FFT (fast-Fourier-transform) convolution integral, as was done in our original NF paper.²¹

Dielectrics are ubiquitous however in nanostructures. We therefore extend here NF to include an arbitrary number of dielectrics by solving the Poisson equation using conjugate gra-

dients. With the modified NF approach, the optical response of any sub-wavelength metal-dielectric system can now be studied. To test the efficiency and accuracy of the method, we first study the optical response of a gold nanoparticle in vacuum and dielectric medium. Then, as an application, we design an Ag nanostructure for the optical detection of a lipid (i.e., dielectric) layer in water. The calculation details the optical response sensitivity to the dielectric coefficient of the lipid, so the designed structure may be a suitable model device for biological probing.

The paper is organized as follows. The NF formalism with the conjugate gradient extension is described in Sec. II. We then present the numerical results for benchmark systems and designed probing nanostructures in Sec. III. Discussion and conclusions follow in Secs. IV and V, respectively.

II. METHODOLOGY

A. Permittivities

Just like in Maxwell descriptions, NF assumes that the dielectric permittivity of a metal can be represented as a sum of Lorentzian oscillators,

$$\epsilon(\mathbf{r}, \omega) = \epsilon_{\infty}(\mathbf{r}) + \epsilon_0 \sum_{j=1}^N \frac{\beta_j(\mathbf{r})}{\bar{\omega}_j^2(\mathbf{r}) - i\alpha_j(\mathbf{r})\omega - \omega^2}. \quad (1)$$

Here, $\epsilon_{\infty}(\mathbf{r})$ is the material-dependent frequency-independent term. For metals, we can adopt $\epsilon_{\infty}(\mathbf{r}) = \epsilon_0$. The material-dependent Lorentzian parameters $\alpha_j(\mathbf{r})$, $\beta_j(\mathbf{r})$, and $\bar{\omega}_j(\mathbf{r})$ are real-valued and N is the number of Lorentzian oscillators. Instead of using the typical number of oscillators $N \sim 2 - 4$ (Ref. 23), we apply up to 9 oscillators to fit the permittivity over a wide frequency range (0.6 \sim 6.7 eV) (Ref. 21).

^{a)}dxn@chem.ucla.edu.

The reason is that due to the large time step, the fitted absorption and natural frequencies (α_j and $\bar{\omega}_j$) cannot be too large, so a larger number of terms is needed to fit, with the added benefit that the fits are now very accurate.

Equation (1) is also formally appropriate for dielectrics. Unlike metals, for near-IR to near-UV frequencies the permittivity of most dielectrics is usually close to a real-valued constant, so it can be represented by a real frequency-independent term,

$$\epsilon(\mathbf{r}, \omega) = \epsilon_\infty(\mathbf{r}),$$

where generally $\epsilon_\infty(\mathbf{r}) > 0$, so that there are no Lorentzian oscillator terms for dielectrics ($\beta_j = 0$ in the dielectric region).

B. Near-field equations

As demonstrated in our previous work, NF is essentially the time-dependent version of the frequency-dependent Poisson algorithm, where one solves

$$\nabla \cdot (\epsilon(\mathbf{r}, \omega) \tilde{\mathbf{E}}(\mathbf{r}, \omega)) = 0. \quad (2)$$

Here, $\tilde{\mathbf{E}}(\mathbf{r}, \omega)$ is the total electric field. To solve this equation in the time domain we introduce, as in Maxwell finite-difference time domain (FDTD), approaches the metallic polarization and current density:

$$\tilde{\mathbf{P}}_p(\mathbf{r}, \omega) = (\epsilon(\mathbf{r}, \omega) - \epsilon_\infty(\mathbf{r})) \tilde{\mathbf{E}}(\mathbf{r}, \omega), \quad (3)$$

$$\tilde{\mathbf{J}}_p(\mathbf{r}, \omega) = -i\omega(\epsilon(\mathbf{r}, \omega) - \epsilon_\infty(\mathbf{r})) \tilde{\mathbf{E}}(\mathbf{r}, \omega), \quad (4)$$

where ‘‘p’’ denotes that this is a metallic (‘‘plasmonic’’) contribution. Using the Lorentzian-oscillators representation of the permittivity in Eq. (1), the time-dependent polarization and current density in the metal evolve as (with $j = 1, \dots, N$)

$$\frac{\partial \mathbf{P}_j(\mathbf{r}, t)}{\partial t} = \mathbf{J}_j(\mathbf{r}, t), \quad (5)$$

$$\frac{\partial \mathbf{J}_j(\mathbf{r}, t)}{\partial t} = -\alpha_j(\mathbf{r}) \mathbf{J}_j(\mathbf{r}, t) - \bar{\omega}_j^2(\mathbf{r}) \mathbf{P}_j(\mathbf{r}, t) + \epsilon_0 \beta_j(\mathbf{r}) \mathbf{E}(\mathbf{r}, t), \quad (6)$$

and the metallic polarization and current density are defined as

$$\mathbf{P}_p(\mathbf{r}, t) = \sum_{j=1}^{N_j} \mathbf{P}_j(\mathbf{r}, t), \quad (7)$$

and

$$\mathbf{J}_p(\mathbf{r}, t) = \sum_{j=1}^{N_j} \mathbf{J}_j(\mathbf{r}, t). \quad (8)$$

Equations (5) and (6) are propagated by the leapfrog algorithm,

$$\mathbf{P}_j(\mathbf{r}, t + dt) = \mathbf{P}_j(\mathbf{r}, t) + dt \mathbf{J}_j\left(\mathbf{r}, t + \frac{dt}{2}\right) \quad (9)$$

and

$$\begin{aligned} \mathbf{J}_j\left(\mathbf{r}, t + \frac{dt}{2}\right) &= \frac{1 - \frac{\alpha_j(\mathbf{r})}{2} dt}{1 + \frac{\alpha_j(\mathbf{r})}{2} dt} \mathbf{J}_j\left(\mathbf{r}, t - \frac{dt}{2}\right) \\ &\quad - \frac{dt}{1 + \frac{\alpha_j(\mathbf{r})}{2} dt} (\bar{\omega}_j^2(\mathbf{r}) \mathbf{P}_j(\mathbf{r}, t) \\ &\quad - \epsilon_0 \beta_j(\mathbf{r}) \mathbf{E}(\mathbf{r}, t)), \end{aligned} \quad (10)$$

with the initial conditions

$$\mathbf{P}_j(\mathbf{r}, t = 0) = \mathbf{J}_j\left(\mathbf{r}, t = -\frac{dt}{2}\right) = 0.$$

Equation (10) is similar to the treatment of the permittivity in Maxwell approaches; the differences come in the representation of the electric field. In the Maxwell FDTD approach, the electric field is propagated as an independent variable, while in NF it is obtained from the overall polarization as follows. From Eqs. (2) and (3) it follows that

$$\nabla \cdot (\mathbf{P}_p + \epsilon_\infty(\mathbf{r}) \mathbf{E}) = 0,$$

and since this equation also holds in the time domain, we can define an individual metallic charge density as

$$\rho_p = -\nabla \cdot \mathbf{P}_p(\mathbf{r}, t). \quad (11)$$

The NF ansatz is that the electric field is a sum of an external field and a transverse induced part,

$$\mathbf{E}(\mathbf{r}, t) = -\nabla \varphi(\mathbf{r}, t) + \mathbf{E}_{\text{ext}}(\mathbf{r}, t), \quad (12)$$

resulting at

$$-\nabla \cdot (\epsilon_\infty(\mathbf{r}) \nabla \varphi(\mathbf{r}, t)) = \rho_p(\mathbf{r}, t) - \nabla \cdot (\epsilon_\infty(\mathbf{r}) \mathbf{E}_0) \delta(t), \quad (13)$$

where we typically use a spatially uniform impulse, i.e.,

$$\mathbf{E}_{\text{ext}}(\mathbf{r}, t) = \mathbf{E}_0 \delta(t).$$

As mentioned, for purely metals-vacuum systems $\epsilon_\infty(\mathbf{r}) = \epsilon_0$ so Eq. (13) then boils down to the Poisson equation, $-\nabla^2 \varphi(\mathbf{r}, t) = \rho(\mathbf{r}, t)/\epsilon_0$, which is easily solved by convolution. However, for dielectrics Eq. (13) is not trivial. To solve it we divide the potential to two parts, labeled qualitatively as dielectric and metallic

$$\phi(\mathbf{r}, t) = \delta(t) \phi_d(\mathbf{r}) + \phi_p(\mathbf{r}, t),$$

where

$$\phi_p(\mathbf{r}, t = 0) = 0,$$

and we note that in practice the delta function in time is represented as

$$\delta(t = ndt) = \begin{cases} 0 & n > 0 \\ \frac{1}{dt} & n = 0. \end{cases}$$

The two potentials fulfill then

$$-\nabla \cdot (\epsilon_\infty(\mathbf{r}) \nabla \varphi_d(\mathbf{r})) = -\nabla \cdot (\epsilon_\infty(\mathbf{r}) \mathbf{E}_0) \quad (14)$$

and

$$-\nabla \cdot (\epsilon_\infty(\mathbf{r}) \nabla \varphi_p(\mathbf{r}, t)) = \rho_p(\mathbf{r}, t). \quad (15)$$

To summarize this section: at $t = 0$, the Poisson equation for the dielectric part (Eq. (14)) is solved; the electric field at $t = 0$ is then obtained from Eq. (12), the result multiplied by $1/dt$, and then Eqs. (9), (10), (12) and (15) are propagated in time.

C. Conjugate gradient solution of the Poisson equation

The only remaining issue is the solution of Eqs. (14) (for $t = 0$) and (15) (for $t > 0$) which are of the general form

$$\hat{A}\phi = \rho, \quad (16)$$

where

$$\hat{A} \equiv -\nabla \cdot (\epsilon(\mathbf{r}) \nabla). \quad (17)$$

Since usually $\epsilon_\infty(\mathbf{r}) > 0$, the matrix representation of operator $-\nabla \cdot (\epsilon(\mathbf{r}) \nabla)$ is positive-definite, and Eq. (17) is therefore easily solved by an iterative conjugate gradient (CG) method²⁴ as follows.

We start from a guess of $\varphi^{(0)}$ (generally vanishing potential). Suppose at step i , we have an approximate solution $\varphi^{(i)}$; the residual or the difference from the correct electron density is defined as

$$r^{(i)} = \rho - \hat{A}\varphi^{(i)}. \quad (18)$$

If we have arrived at the exact solution, the residual will vanish, i.e.,

$$\int |r^{(i)}|^2 \approx 0, \quad (19)$$

and otherwise we try to update the solution with the conjugate searching direction vector $p^{(i)}$ (starting with $p^{(0)} = r^{(0)}$) and a scalar coefficient $\alpha^{(i)}$, calculated from

$$\alpha^{(i)} = \frac{\int |r^{(i)}|^2}{\int p^{(i)T} A p^{(i)}}. \quad (20)$$

The solution is updated as

$$\varphi^{(i+1)} = \varphi^{(i)} + \alpha^{(i)} p^{(i)}, \quad (21)$$

and the corresponding residual is now

$$r^{(i+1)} = \rho - \hat{A}\varphi^{(i+1)} = r^{(i)} - \alpha^{(i)} \hat{A} p^{(i)}. \quad (22)$$

The conjugate searching direction will also be updated,

$$p^{(i+1)} = r^{(i+1)} + \beta^{(i)} p^{(i)}, \quad (23)$$

with the scalar ratio $\beta^{(i)}$ given by

$$\beta^{(i)} = \frac{\int |r^{(i+1)}|^2}{\int |r^{(i)}|^2}. \quad (24)$$

With a sufficient number of iteration steps, we can reach the solution of the Poisson equation with an arbitrary accuracy. In our implementation, the convergence criterion is set as $\int |r^{(i)}|^2 d^3\mathbf{r} < 10^{-5} \int \rho_0^2 d^3\mathbf{r}$, where we introduce the density at $t = 0$. With this criterion, the convergence is to the same absolute magnitude at all times. At the latter propagation times, when the density term in the Poisson equation is smaller, fewer iteration steps are sufficient to reach the same absolute error (with larger relative errors, of course). The number of

iteration steps is further reduced at late times since the solution for the $\phi(ndt)$ is used as the starting solution for $\phi((n+1)dt)$. Taken together, these two facts lead to a reduction in the number of iteration steps as a function of time (from about 60 initially to about 20 later on, as mentioned below).

III. RESULTS

We test the dielectrics-enabled version of NF for two benchmarks involving gold and silver. The fit of the metallic Lorentzian parameters to experimental values²⁵ is taken from our previous work.²¹ We first test gold spherical nanoparticles in vacuum and silica. Then we study the sensitivity of silver nanostructures for optical detection of a lipid layer in water. In all simulations, the conjugate-gradient solution converged rather quickly; typically up to 60 conjugate iterations were used at the beginning, but as one propagates in time, the number of conjugate gradient steps is reduced, so in average we use about 20 iterations per time step.

A. Absorption efficiency

In all simulations below, the optical properties are determined by the absorption coefficient, defined as

$$Q_{\text{ext}} = \frac{1}{\pi a^2} \cdot \frac{4\pi\omega}{nc} \int \text{Im}(\tilde{\mathbf{P}}(\mathbf{r}, \omega) \cdot \mathbf{E}_0) d^3\mathbf{r}. \quad (25)$$

Here, a is the radius of the spherical particle, n is the refractive index of the surrounding medium, and $\tilde{\mathbf{P}}(\mathbf{r}, \omega)$ is the frequency-dependent total polarization defined as

$$\tilde{\mathbf{P}}(\mathbf{r}, \omega) = \tilde{\mathbf{P}}_p(\mathbf{r}, \omega) + (\epsilon_\infty(\mathbf{r}) - \epsilon_b) \tilde{\mathbf{E}}(\mathbf{r}, \omega),$$

where

$$\tilde{\mathbf{E}}(\mathbf{r}, \omega) \equiv \int \exp(i\omega t) \mathbf{E}(\mathbf{r}, t) dt = -\nabla \tilde{\phi}(\mathbf{r}, \omega) + \mathbf{E}_0,$$

and the frequency-dependent polarization and densities are similarly defined. In Eq. (25), we introduce $\epsilon_b \equiv \epsilon_0 n^2$. Finally, in some of the simulations below we use a non-spherical system (sphere+rod), but for simplicity keep the same prefactor definition, i.e., use only the cross-section area (πa^2) of the sphere in the prefactor in Eq. (25). Also note that we use the term absorption and extinction interchangeably here, since NF has no retardation and therefore no scattering, so the extinction and absorption coefficients are equal.

B. Spherical nanoparticle in vacuum

We first study a spherical particle in vacuum. We studied such systems in our previous work which developed the NF technique,²¹ but we repeat the simulations since we replace the Fourier-transform convolution²¹ for the Poisson equation by conjugate gradients. The radius of each particle is set as $a = 5$ nm, but the method is invariant to overall scale change as it is an NF approach. A uniform grid spacing ($dx = dy = dz = 0.25$ nm) was used with a cubic box of $(L = 16 \text{ nm})^3$. The time-step is $dt = 2$ a.u. ~ 0.05 fs and Eqs. (9), (10), (12) and (15) were propagated for several thousand atomic units till convergence.

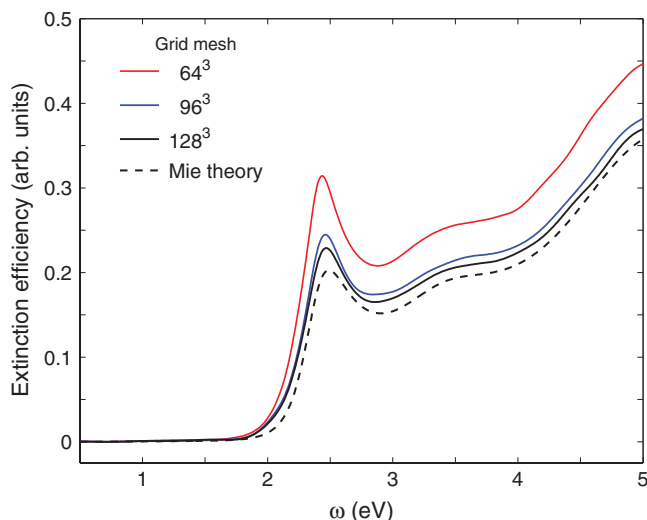


FIG. 1. Near-field calculation of extinction (absorption) efficiency for an Au spherical nanoparticle in vacuum (solid lines). The particle radius is 5 nm, and the simulation spacing is $\Delta x = 0.25$ nm. With increasing box size, the NF result approaches the Mie scattering spectrum (the dashed line). The results are labeled by the number of grid points in each dimension, so they correspond to grid sizes of $L = 16$ - 32 nm; for comparison, the particle diameter is 10 nm.

Figure 1(a) gives the calculated Q_{ext} as a function of frequency. The spectrum shows a major response at 2.4 eV due to the dipole surface plasmon resonance. For a bigger box size ($L = 32$ nm), with the same spacing, the spectrum is similar and shifted down in magnitude approaching closer the analytical Mie theory limit which should be achieved for $L \rightarrow \infty$, $dx \rightarrow 0$. One way to view the box size dependence is that for large boxes there is less interaction between dipoles at periodic images of the cell; alternately, we can view the dependence as emerging from reflection of the field near the edges and this implies that perhaps analytical continuation approaches such as perfectly matched layers will allow the use of smaller boxes.

C. Nanoparticle embedded in silica

We further apply the approach to study the optical absorption efficiency for a gold nanoparticle embedded in silica, a nanostructure which is well studied both theoretically and experimentally.^{9,26,27} For optical frequencies, the dielectric permittivity of silica is almost a constant, so we use a frequency-independent term $\epsilon_{\text{SiO}_2} = 2.25\epsilon_0$. The calculation is similar to the previous spheres-in-vacuum example, but we found that a somewhat smaller grid spacing (0.167 nm) was necessary here.

Figure 2 gives the calculated extinction (i.e., absorption) efficiency of gold a nanoparticle embedded in silica. The spectrum shows a plasmon resonance around 2.0 eV, red-shifted from 2.4 eV when in vacuum, as in Fig. 1(a). When increasing the simulation box, the plasmon resonance blueshifts, approaching again the exact Mie calculation result in the dashed line. Also note that there is a small artificial peak around $\omega = 1.9$ eV, which is a finite dx effect (more specifically, at a finite dx there are artificial spatial edges which

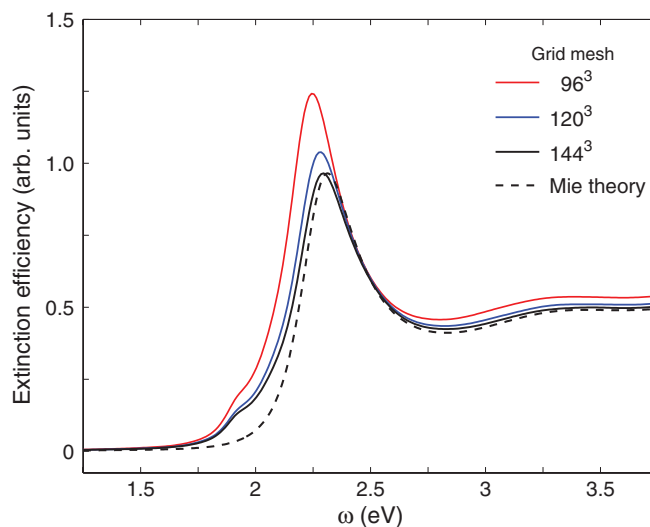


FIG. 2. NF calculation of the extinction (absorption) efficiency of an Au nanoparticle embedded in silica ($\epsilon_{\text{SiO}_2} = 2.25\epsilon_0$). The particle radius is again 5 nm while the grid spacing is $\Delta x = 0.167$ nm. With increasing box size, the NF results approach Mie theory (dashed line) except for a small peak around 1.9 eV which disappears when dx is smaller (not shown).

emerge when a sphere is described in a 3D Cartesian coordinate system, and the large field at these edges modifies the overall peak structure).

D. Nanostructures for detection of a flexible lipid layer

Inspired by the tunability of the surface plasmon resonance by the metal-dielectric interface, we studied the spectrum of a lipid layer in water, and tested the sensitivity of the spectrum to the dielectric constant of the lipid and therefore to the presence of the layer. Such a system could be considered as a simple example for dielectric-induced photodetection of a dielectric lipid layer's presence.

Figure 3 shows the designed probing nanostructures, a single silver sphere and a silver sphere+rod combination. The system is immersed in water. A lipid layer, when present, is assumed to wrap around the sphere but not the rod.

The layer is modeled as a dielectric shell with an outer radius of 5 nm. In the sphere+rod combination, the latter is cylindrical with length 7 nm. Two rod diameters were studied, 1 nm and 2 nm. For the sphere+rod system, we studied both perpendicular and parallel polarizations. The permittivity of water is taken as $\epsilon_{\text{H}_2\text{O}} = 1.8\epsilon_0$, and for the lipid $\epsilon_{\text{lipid}} = 2.2\epsilon_0$. The box size was the same ($L = 16$ nm) as in the pure sphere case. The grid mesh is as dense as $128 \times 128 \times 128$ to get close to converged results.

Figure 4(a) shows the optical response of a silver spherical particle with and without a lipid layer attached. The major peak at 3.3 eV of an isolated Ag particle in water is redshifted to 3.15 eV when the lipid layer is attached. This resonance comes from the dipole surface plasmon at the spherical metal-water interface.

We then study (Fig. 4(b)) the sphere+rod system for a rod with diameter $d = 1$ nm. When the incoming light is polarized perpendicular to the rod, the response is similar to that in an isotropic spherical particle, so that when the lipid

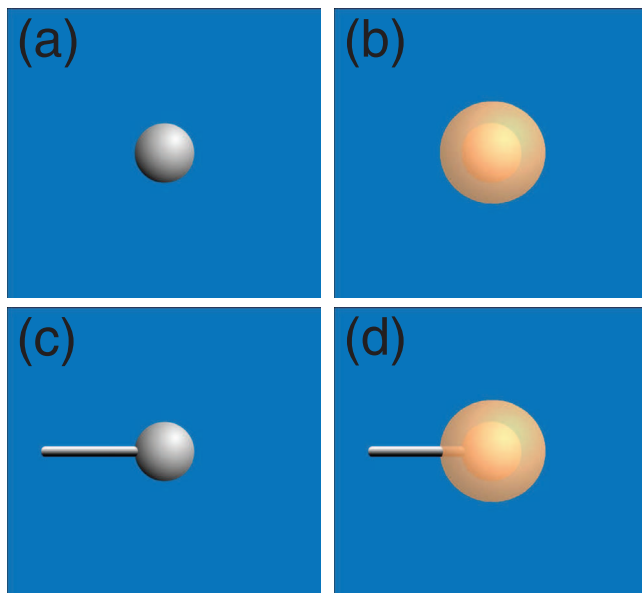


FIG. 3. Schematic illustrations of an Ag nanostructure for the optical detection of a lipid layer in water. (a) A single Ag nanoparticle with diameter 6 nm in water and (b) with lipid layer surrounded. (c-d) like (a-b), but now a rod of length 7 nm is attached on the sphere.

layer wraps around the sphere the major resonance is redshifted by ~ 0.15 eV. With the light polarization parallel to the rod, another mode appears at ~ 1 eV due to the plasmonic resonances at the rod end. But the major resonance at 3.3 eV still survives and when lipid layer is attached it redshifts again to ~ 3.15 eV. Note that even for this small mesh ($dx = 0.125$ nm), the calculation is not fully converged with dx due to the small rod size (1 nm), leading to an artificial split of the low-frequency feature.

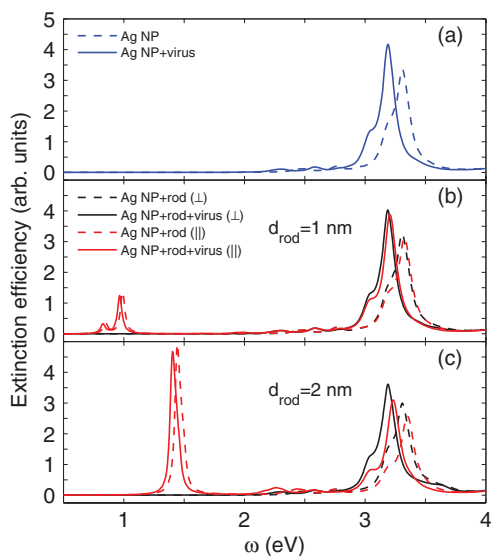


FIG. 4. Calculated extinction (absorption) efficiency of the different nanostructures in Fig. 3, using $\epsilon_{\text{H}_2\text{O}} = 1.8\epsilon_0$ and $\epsilon_{\text{lipid}} = 2.2\epsilon_0$. Panel (a) shows the optical response before and after the Ag nanoparticle is wrapped by the lipid layer. Panel (b) gives the optical response of a complex nanostructure (sphere+rod with rod diameter 1 nm) before and after lipid adsorption. Both parallel and perpendicular polarizations are studied. (The splitting of the two peaks at low frequencies in panel (b) is an artifact due to finite grid discretization.) Panel (c) is similar to (b), but for $d = 2$ nm.

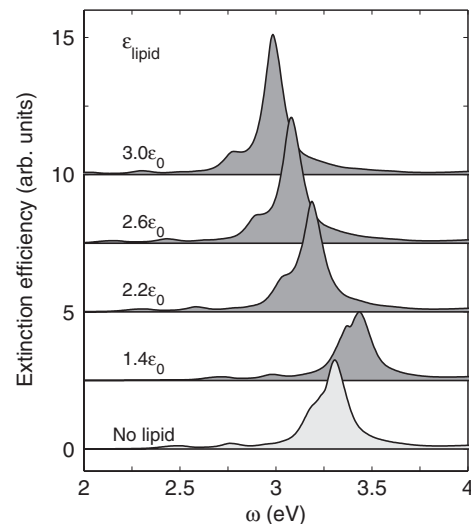


FIG. 5. The evolution of the optical response of a bare and wrapped (shaded areas) Ag sphere+rod structure, as a function of the dielectric constant of the wrapping lipid layer. Here the light polarization is perpendicular to the rod.

The results for a thicker rod (diameter 2 nm) before and after lipid wrapping are given in Fig. 4(c). As before the resonance above 3 eV is shifted down by 0.15 eV, while due to the smaller aspect ratio of the rod the parallel plasmon mode is now at a higher frequency around 1.4-1.5 eV and is again sensitive (by a shift of ~ 0.1 eV) to the presence of the lipid layer.

Note that there are multiple peaks around 1.4 and 1.5 eV. In essence, this is because the sphere splits the parallel plasmon mode.

To further investigate the optical sensitivity of a dielectric wrapped sphere+rod system to the dielectric constant, we performed a series of calculations in Fig. 5. The layer permittivity is varied gradually from $1.4\epsilon_0$ to $3.0\epsilon_0$, and the light polarization is perpendicular to the rod. For a layer permittivity of $1.4\epsilon_0$, the response of attached structure is blueshifted with respect to the unattached due to the smaller permittivity of the lipid compared to water. But with increasing layer permittivity, the resonance peak continues to redshift. The results demonstrate the sensitivity of optical response of nanostructures to the dielectric property of the layer. Since the results are scale independent in the sub-wavelength limit, structures in the ranges of 2-100 nm could potentially benefit from such detection.

IV. DISCUSSION

The CG method used here is very efficient in solving the generalized Poisson equation, and the calculation can be further accelerated if preconditioning is used. We also note that at this stage, CG the based method is limited to dielectrics with $\epsilon_\infty(\mathbf{r}) > 0$, since only with this condition could $-\nabla \cdot (\epsilon(\mathbf{r})\nabla)$ be positive-definite. However, plasmonics of metallic nanostructures in contact with metamaterials or gain media with $\epsilon_\infty(\mathbf{r}) < 0$ are also of great interests. One future goal is to enable the NF method to include materials with negative dielectric function. This could be achieved, e.g., by solving the Poisson equation self-consistently, i.e., by an

iterative solution of

$$-\nabla^2\phi(\mathbf{r}, t) = \frac{\rho_p(\mathbf{r}, t)}{\epsilon_0} + \nabla \cdot \left(\frac{\epsilon_\infty(\mathbf{r}) - \epsilon_0}{\epsilon_0} \nabla\phi(\mathbf{r}, t) \right).$$

V. CONCLUSIONS

In conclusion, we extended NF electrostatics to include dielectrics. Using CG, the non-trivial generalized Poisson equation in the NF formalism is economically solved with arbitrary accuracy, and the numerical effort is comparable to the integral convolution method which was previously used by us for non-dielectrics (i.e., metals+vacuum). The new approach is applied to study the optical response of metallic spherical nanoparticles in dielectrics. The benchmark results are in good agreement with analytical Mie scattering.

As an application of the dielectrics-enabled NF method, we designed a silver nanoparticle based structure for the optical detection of a wrapped lipid layer in water. The calculations show that the major optical response of nanostructure is mostly sensitive to the dielectric properties of the layer, as well as to the polarization. Such structures could potentially be applied for detection and characterization of absorbed lipid layers.

Finally, with ordinary dielectrics included in the NF method, it is now a powerful tool which can be widely used to study near-field optics in various metal-dielectric nanostructures. Applications for embedding with the time-dependent Schrödinger equation for molecules will be discussed in future works.

ACKNOWLEDGMENTS

We are grateful for support by the National Science Foundation (NSF), Grant No. CHE-1112500.

- ¹L. Novotny and B. Hecht, *Principles of Nano-Optics* (Cambridge University Press, Cambridge/New York, 2006).
- ²S. A. Maier, *Plasmonics: Fundamentals and Applications* (Springer, New York, 2007).
- ³N. J. Halas, *Nano Lett.* **10**, 3816 (2010).
- ⁴K. A. Willets and R. P. Van Duyne, *Annu. Rev. Phys. Chem.* **58**, 267 (2007).
- ⁵J. N. Anker, W. P. Hall, O. Lyandres, N. C. Shah, J. Zhao, and R. P. Van Duyne, *Nature Mater.* **7**, 442 (2008).
- ⁶E. Ozbay, *Science* **311**, 189 (2006).
- ⁷S. Linic, P. Christopher, and D. B. Ingram, *Nature Mater.* **10**, 911 (2011).
- ⁸A. Kim, F. S. Ou, D. A. A. Ohlberg, M. Hu, R. S. Williams, and Z. Y. Li, *J. Am. Chem. Soc.* **133**, 8234 (2011).
- ⁹E. Prodan, C. Radloff, N. J. Halas, and P. Nordlander, *Science* **302**, 419 (2003).
- ¹⁰E. Prodan and P. Nordlander, *J. Chem. Phys.* **120**, 5444 (2004).
- ¹¹J. M. McMahon, S. K. Gray, and G. C. Schatz, *Phys. Rev. Lett.* **103**, 097403 (2009).
- ¹²J. M. McMahon, S. K. Gray, and G. C. Schatz, *Phys. Rev. B* **82**, 035423 (2010).
- ¹³Y. Sivan, S. M. Xiao, U. K. Chettiar, A. V. Kildishev, and V. M. Shalaev, *Opt. Express* **17**, 24060 (2009).
- ¹⁴D. J. Masiello and G. C. Schatz, *Phys. Rev. A* **78**, 042505 (2008).
- ¹⁵H. N. Chen, J. M. McMahon, M. A. Ratner, and G. C. Schatz, *J. Phys. Chem. C* **114**, 14384 (2010).
- ¹⁶D. Neuhauser and K. Lopata, *J. Chem. Phys.* **127**, 154715 (2007).
- ¹⁷K. Lopata and D. Neuhauser, *J. Chem. Phys.* **130**, 104707 (2009).
- ¹⁸K. Lopata and D. Neuhauser, *J. Chem. Phys.* **131**, 014701 (2009).
- ¹⁹C. Arntsen, K. Lopata, M. R. Wall, L. Bartell, and D. Neuhauser, *J. Chem. Phys.* **134**, 084101 (2011).
- ²⁰D. Neuhauser, *J. Chem. Phys.* **135**, 204305 (2011).
- ²¹A. Coomar, C. Arntsen, K. A. Lopata, S. Pistinner, and D. Neuhauser, *J. Chem. Phys.* **135**, 084121 (2011).
- ²²A. Taflove and S. C. Hagness, *Computational Electrodynamics : The Finite-Difference Time-Domain Method*, 3rd ed. (Artech House, Boston, 2005).
- ²³F. Hao and P. Nordlander, *Chem. Phys. Lett.* **446**, 115 (2007).
- ²⁴W. H. Press, *Numerical Recipes in Fortran 77 : The Art of Scientific Computing*, 2nd ed. (Cambridge University Press, Cambridge, England/New York, 1996).
- ²⁵P. B. Johnson and R. W. Christy, *Phys. Rev. B* **6**, 4370 (1972).
- ²⁶N. J. Halas, *MRS Bull.* **30**, 362 (2005).
- ²⁷C. Radloff and N. J. Halas, *Appl. Phys. Lett.* **79**, 674 (2001).